




# Defect-driven relaxation of nanostructured Cu examined by in situ heating high-energy synchrotron X-ray microbeam diffraction

Isshu Lee<sup>a,b</sup>, Laxman Bhatta<sup>a,b</sup>, Donghua Xu<sup>a,b</sup>, Malte Blankenburg<sup>c</sup>, Ulrich Lienert<sup>c</sup>, Klaus-Dieter Liss<sup>d,\*</sup>, Megumi Kawasaki<sup>a,b,\*\*</sup> 

<sup>a</sup> Materials Science Program, Oregon State University, Corvallis, OR 97331, USA

<sup>b</sup> School of Mechanical, Industrial and Manufacturing Engineering, Oregon State University, Corvallis, OR 97331, USA

<sup>c</sup> Deutsches Elektronen-Synchrotron (DESY), Hamburg 22607, Germany

<sup>d</sup> University of Tennessee, Oak Ridge Innovation Institute, Knoxville, TN 37996, USA

## ARTICLE INFO

### Keywords:

Copper  
High-pressure torsion  
Line broadening  
Nanocrystalline metal  
Recrystallization  
Synchrotron radiation

## ABSTRACT

Bulk nanostructured metals introduced by severe plastic deformation contain an excess of lattice defects. A nanostructured copper (Cu) processed by a high-pressure torsion technique was examined during in situ heating to investigate microstructural relaxation and quantify the evolution of microstructural parameters using high-energy synchrotron microbeam X-ray diffraction. While general microstructural relaxations, such as recovery, recrystallization, and subsequent grain growth, were observed, the key microstructural parameters, including grain size, microstrain, dislocation density, and thermal expansion coefficient, and their changes at critical temperatures were uniquely described and quantified through diffraction data. Based on this analysis, the stored energies driving thermally activated microstructural changes were estimated for individual defect types — grain boundaries, dislocations, and vacancies — that are expected to significantly influence the relaxation behavior of nanostructured Cu. This study demonstrates the effectiveness of diffraction characterization techniques for gaining a comprehensive understanding of the thermal stability of bulk nanostructured materials.

## 1. Introduction

Severely deformed nanostructured metals were investigated largely due to the uniquely formed nanostructures with a significant density of defects, such as very high dislocation densities at non-equilibrium grain boundaries [1,2]. These energetic microstructures raise further scientific questions about the thermal stability of nanostructures. Quantifying vacancies has been challenging due to the difficulty in separating their contributions from other lattice defects. However, several indications of excess lattice vacancies emerged after comprehensively characterizing defect structures in nanocrystalline pure metals and alloys, i.e. copper (Cu), using various analytical techniques, including X-ray diffraction (XRD), transmission electron microscopy (TEM), electrical resistivity, dilatometry and differential scanning calorimetry (DSC) [3], and positron annihilation spectroscopy [4,5]. The results from different experiments yielded reasonably consistent estimations of excess vacancy with a concentration of  $10^{-4}$ – $10^{-3}$  [3,4], which is 7–8 orders of magnitude higher than the equilibrium concentration of relaxed metallic materials

at room temperature. By contrast, such high vacancy concentrations can only be thermally activated at temperatures close to the melting point of metallic materials.

Heat treatments applied to plastically strained bulk nanostructured metals can facilitate the annihilation of dislocations through diffusion-driven recovery and recrystallization processes. The thermal stability of the nanostructure is crucial for maintaining the improved mechanical properties associated with nanostructure [6]. This understanding is vital for developing new materials. However, a comprehensive evaluation of the sequential thermal behavior of nanostructured metals, which possess a high density of defects, remains a complex and challenging issue.

Accordingly, this study was initiated to understand defect-driven microstructural relaxation from nanostructure in a simple metal of copper (Cu) through a novel X-ray microbeam diffraction technique upon heating. By capturing the evolution of nanostructure with excess defects in a bulk volume, the resulting microstructural data will be used to evaluate the critical temperature for microstructural relaxation and estimate the driving force behind thermal recovery events in

\* Corresponding author.

\*\* Corresponding author at: Materials Science Program, Oregon State University, Corvallis, OR 97331, USA.

E-mail addresses: [kdl@utk.edu](mailto:kdl@utk.edu) (K.-D. Liss), [megumi.kawasaki@oregonstate.edu](mailto:megumi.kawasaki@oregonstate.edu) (M. Kawasaki).

<https://doi.org/10.1016/j.jalcom.2025.180599>

Received 7 December 2024; Received in revised form 21 March 2025; Accepted 23 April 2025

Available online 24 April 2025

0925-8388/© 2025 Elsevier B.V. All rights are reserved, including those for text and data mining, AI training, and similar technologies.

nanostructured Cu.

## 2. Experimental material and procedures

A cylindrical bar of commercial purity Cu (>99.5 % purity) with a 10 mm diameter was sliced into circular disks having  $\sim 0.85$  mm thicknesses. Grain refinement was conducted on the Cu disks through high-pressure torsion (HPT) at room temperature (300 K) under 6 GPa for 15 turns at 1 rpm. Such a high torsional turn under 6 GPa is sufficient to introduce homogeneous nanostructures in simple metals [7]. In situ heating observation was conducted using microbeam high-energy synchrotron X-ray diffraction at the PETRA-III beamline P21.2 at DESY to evaluate the microstructure evolution and relaxation upon heating. A constant temperature increase of 0.1656 K/s was programmed from room temperature of 300 K to 873 K followed by holding for 56 s and furnace cooling. The beam with a fixed incident wave vector of  $k = 31.27 \text{ \AA}^{-1}$  illuminated a cross-section of about  $6 \times 3 \text{ \mu m}^2$  and through the disk thickness of the sample of  $\sim 700 \text{ \mu m}$ . The microbeam measurement location was in a saturated nanostructure region between half of the disk radius and the disk edge. A detailed experimental procedure, data reduction and acquisition were documented for an experiment conducted on a Mg alloy using the identical setup at the same beamtime [8].

The Cu disk after HPT was examined by TEM, with the focused ion beam-prepared specimen taken  $\sim 4.0$  mm from the disk center to capture the initial microstructure before microbeam X-ray measurements. The TEM image was taken on an FEI Titan using a tilted incident beam dark field technique with 200 keV voltage and a spot size of 6, thus, the electron beam focused on the sample is  $\sim 6$  nm in diameter when acquiring a dark field image. Vickers microhardness was tested on the Cu disk after HPT at 300 K and additional heating to seven arbitrarily selected temperatures followed by quenching, using the same heating ramp under DSC to replicate the microstructure observed in the diffraction experiments at those temperatures. The HPT-processed Cu samples used in this study were prepared only a few days prior to each test to minimize the effects of self-annealing in Cu [9–11].

## 3. Results

### 3.1. Nanostructure before the heating experiment

Fig. 1(a) shows the TEM dark-field image taken across the torsional direction of the Cu disk after HPT for 15 turns. The captured microstructure shows the grains in an equiaxed shape and average sizes of 240–260 nm are estimated. TEM observations revealed the absence of twin boundaries after HPT at room temperature, likely due to the low

processing temperature, as supported by earlier studies [12,13]. This microstructure exhibited a Vickers microhardness of  $H_V = 154 \pm 1$ , approximately three times higher than the hardness of unprocessed Cu of  $H_V = 50$ . The introduced nanostructure and the hardness value agree with the previous reports of bulk nanostructured Cu after HPT [11,14,15]. The nanostructure in Cu serves as the initial microstructural condition for the subsequent in situ heating microbeam high-energy synchrotron X-ray diffraction experiment.

### 3.2. Diffraction data: intensity – scattering vector – time map

The present in situ heating diffraction study was analyzed to yield a color-coded intensity – scattering vector – time map with a temperature-time plot as shown in Fig. 1(b), where 27 reflection peaks in plane coordinates for Cu are listed along the lower x-axis. Based on the 27 reflection peaks of the f.c.c. crystal, no precipitation or phase transformation was observed in the Cu, while new peaks, specifically at low scattering vectors, became visible above 700 K, which are attributed to the formation of oxide  $\text{Cu}_2\text{O}$  [16]. Clear lattice expansion followed by contraction is visible by shifting all diffraction peaks during heating and cooling, respectively. The broadest peak width at 0 s of heating, representing the microstructure after HPT, is expected from the refined grains as displayed in Fig. 1(a). The broadened peaks are reduced with heating. This peak sharpening appears gradually upon heating, while significant narrowing is visible around 480 K and 700 K towards spotty patterns, thereby denoting grain coarsening.

The peak shift during heating was evaluated for all reflection peaks of the Cu sample. The interplanar spacing at 303–332 K was linearly extrapolated to estimate the spacing at 300 K,  $d_0$ , for all 27 separate reflection peaks, and the peak shift yielding the change in the interplanar spacing  $\Delta d$  upon heating enabled the estimation of the lattice strain  $\Delta d/d_0$  up to 873 K. The results are displayed in Fig. 2(a) for all reflection peaks with color keys on the right. Lattice strain plots in separate reflection planes are available in Supplementary Fig. S1. The thermal expansion coefficient of the Cu sample upon heating is computed by taking the slopes of lattice strain against temperature for  $\pm 5$  K spanning a 10 K range around every temperature point on each reflection peak, as shown in Fig. 2(b). An average thermal expansion coefficient of  $17.033 \times 10^{-6} \text{ K}^{-1}$  was calculated at a range of 303–361 K from all 27 peaks of the Cu sample, where this estimation process is described in Fig. 2(c). From Fig. 2(a) and (b), a large scatter of these microstructure-related parameters became apparent at 470–480 K and increased at higher temperatures. Nevertheless, the trend line for the thermal expansion coefficient of Cu is well recognized and increases with temperature, with values consistent with reported data [17].

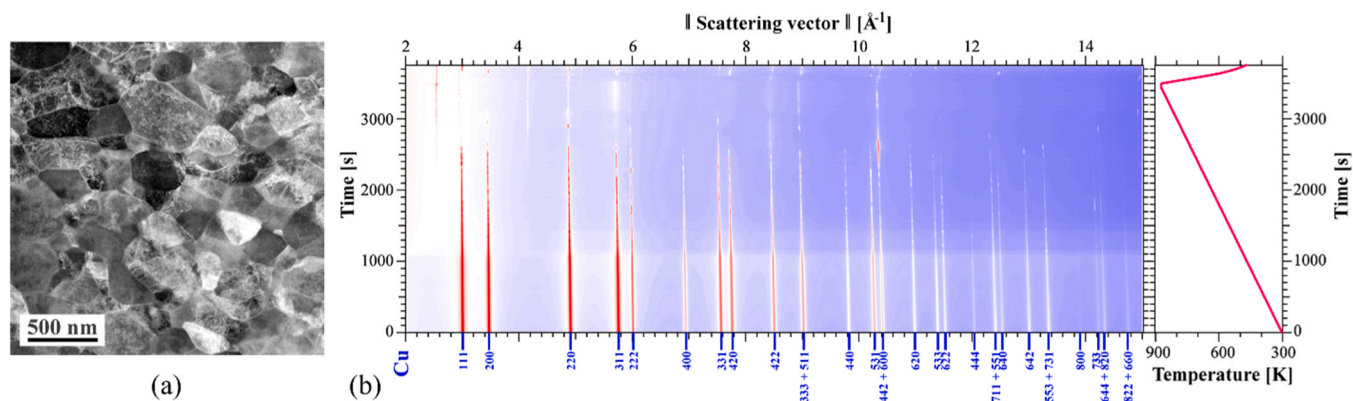


Fig. 1. (a) TEM dark field image of the nanostructured Cu after HPT for 15 turns under 6 GPa, and (b) a color-coded intensity-scattering vector-time map with a temperature-time plot showing the high-energy synchrotron microbeam X-ray diffraction peaks for the nanostructured Cu sample. Miller indices for the f.c.c. Cu are shown.

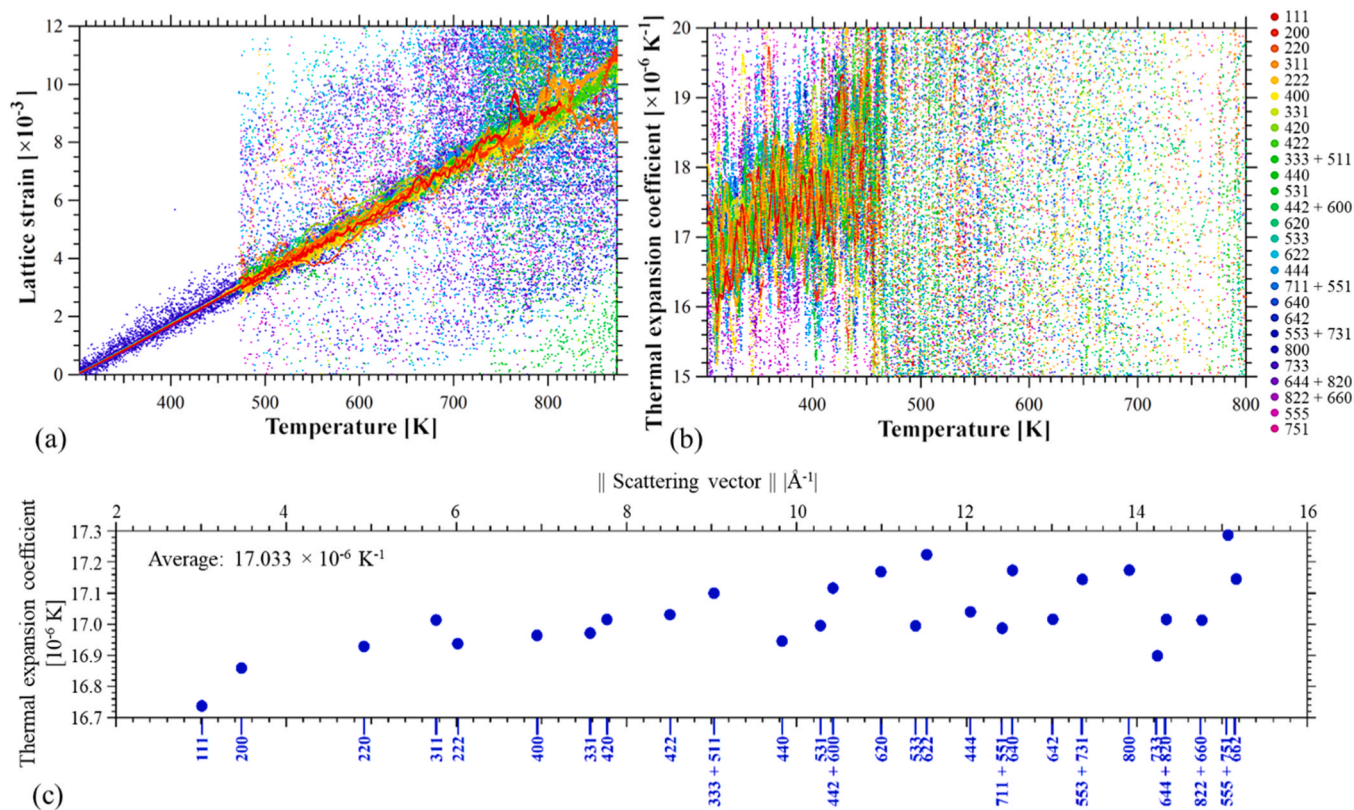


Fig. 2. (a) Lattice strain and (b) thermal expansion coefficient versus temperature plots for the 27 reflection peaks of the Cu sample. The color keys for the peaks are listed on the right.; (c) Thermal expansion coefficient versus scattering vector plot at a range of 303–361 K from the 27 reflection peaks of the Cu sample, estimating an average thermal expansion coefficient of  $17.033 \times 10^{-6} \text{ K}^{-1}$ .

### 3.3. Diffraction data: Azimuth - time plot

To visualize the transition of the sequential defect-driven microstructural relaxation of the nanostructured Cu, the diffraction data of the Cu-111 reflection was described in an azimuth - time and temperature plot in Fig. 3. In this way, the continuous diffraction lines orienting from the nanoscale crystals are discernible as long as the microstructure maintained the nanoscale up to 480 K denoted by yellow dashed lines over the azimuth angles without available diffraction data. Well-distinguishable diffraction spots were visible up to the temperature slightly above 700 K denoted by green dashed lines. This presentation of diffraction data highlights patterns that indicate variations in microstructure. The transition temperatures associated with different diffraction patterns reveal changes in the distinct microstructural behaviors of nanostructured Cu. These results will be used to discuss the variations in grain size, as estimated from the diffraction data, in a later section. The consistent transitions of diffraction spots, such as the change from a continuous to spotty appearance at  $\sim 480$  K followed by

disappearance just above 700 K with increasing temperature, can also be observed in other reflections, i.e., 200, 220, 311, 222, and 400 (see Supplementary Fig. S2) for the nanostructured Cu under heating.

## 4. Discussion

### 4.1. Microstructure transition through the Williamson-Hall analysis

A Williamson-Hall analysis was conducted to evaluate the crystallite size and microstrain, enabling the estimation of dislocation density and its changes upon heating of the nanostructured Cu. Due to the high-energy X-rays providing access to high-order reflections, the influence of unsystematic peak-width versus scattering-vector data, related to the strain anisotropy around dislocations, often encountered in bulk nanostructured materials can be minimized. As a result, the need for additional procedures, such as the modified Williamson-Hall analysis [18, 19], is avoided in this work. Fig. 4(a) shows the Williamson-Hall plot constructed for three representative temperatures providing linear

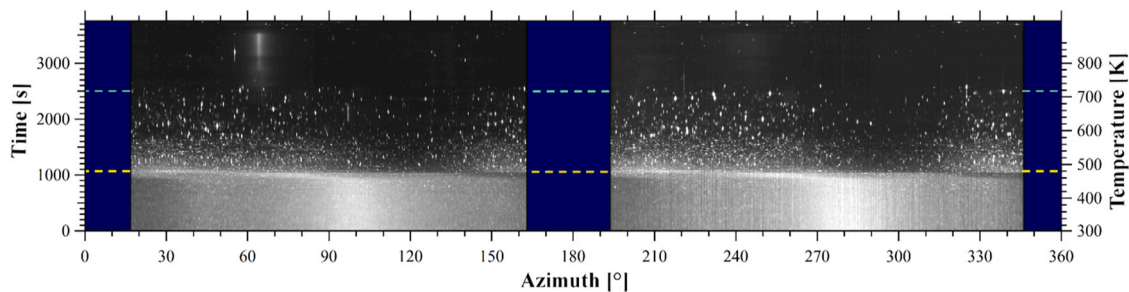


Fig. 3. Azimuth angle - time and temperature plot for the 111 reflection of the Cu sample. Dashed lines indicate specific times and temperatures when the diffraction spot patterns change.

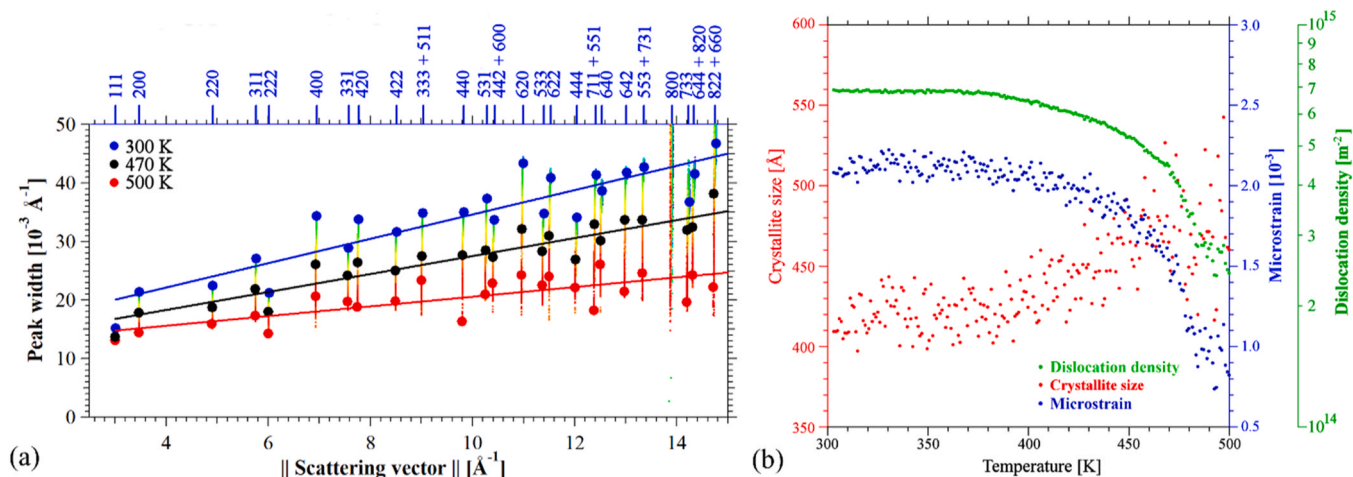


Fig. 4. (a) Williamson-Hall plot taken at 300 K, 470 K, and 500 K and (b) the estimated crystallite size, microstrain, and dislocation density with temperature for the HPT-processed Cu.

trends for computing the microstructure features of the Cu sample with increasing temperature. However, as seen in Fig. 4(a), temperatures around 500 K and above exhibit significant fluctuations in the full width at half maximum (FWHM) across all reflection peaks, making it impossible to estimate the microstructural parameters using a simple relationship between scattering vector  $Q$ , FWHM  $\Delta Q$ , crystallite size  $D$ , and microstrain  $\epsilon$ . Therefore, the microstructure features were estimated using the reliable data available and are shown up to 500 K in Fig. 4(b), where the dislocation density is given by  $\rho = (2\sqrt{3} \langle \epsilon^2 \rangle^{1/2}) / bD$ , [20], with  $b = 2.556 \times 10^{-10} \text{ m}$  taken from the lattice parameter of  $3.614 \text{ \AA}$  at 300 K for the HPT-processed Cu. A trend of maintaining these microstructural features of  $D = 40\text{--}44 \text{ nm}$ ,  $\epsilon > 2.1 \times 10^{-3}$ , and  $\rho = 6.8 \times 10^{14} \text{ m}^{-2}$  after HPT at 300 K through heating to 400 K was followed by slight reductions in dislocation density and microstrain and an increase in crystallite size up to 470 K. The trend is consolidated with increasing temperature. The current in situ heating examination reveals essential details about the time-resolved microstructural relaxation transitions of the nanostructured Cu under heating.

While the in-situ heating high-energy synchrotron X-ray microbeam diffraction experiment provided the essential microstructural evolution from the nanostructure, temperatures above 500 K were not informative due to technical limitations. Further analysis is necessary to continue the grain coarsening linking with grain orientation [8] during the thermal evolution of the nanostructure in Cu.

#### 4.2. Transition temperatures through diffraction-estimated grain size

The diffraction data with time and temperature was reformatted by translating into a scalable microstructural feature of grain size by applying a reported relationship of  $D = (V_g/N_s)^{1/3}$ , where  $V_g$  is the X-ray illumination volume on the Cu sample of  $\sim 1.6 \times 10^4 \text{ \AA}^3$  and  $N_s$  is the number of grains associated with the scattered reflection, which requires a systematic counting of the diffraction spots at each temperature [8]. For instance, for the Cu-111 reflection,  $N_s = (4\pi/\delta^2) \cdot (\delta/\eta/N_m/\cos(\theta)) = 3.3 \times 10^4$  for the nanostructured Cu at 300 K, where the separation angle between spots is  $\delta = 0.34^\circ$  and the mosaic spread of azimuthal width of each spot is  $\eta = 0.47^\circ$ ,  $N_m = 8$  as a multiplicity of the 111 reflection, the Bragg angle  $\theta$  gives  $\cos(\theta) = (1 - Q^2/4k^2)^{1/2}$  with  $Q = 3.010 \text{ \AA}^{-1}$  for the 111 reflection, and  $k$  is the incident wave vector of the X-ray. These calculations were repeated for the first 5 reflection peaks of the Cu (Supplementary Fig. S3) and Fig. 5 displays the average diffraction-data estimated grain sizes (thick black line) with standard deviations (thin black lines) upon heating of the Cu after processing, where the corresponding Vickers microhardness values examined after

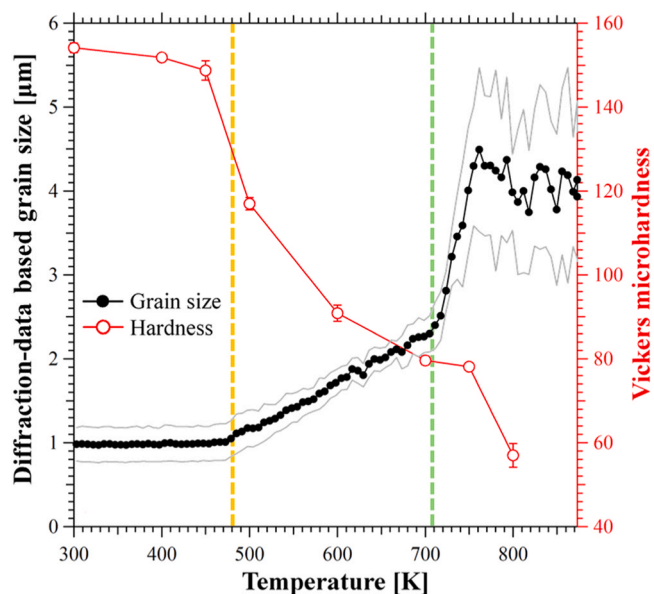


Fig. 5. A plot of the in situ diffraction-data based grain size and ex situ heating Vickers microhardness with increasing temperature of the Cu sample.

replicated heating are superimposed. The critical temperatures at which the diffraction spot patterns had dramatically changed, which are marked in yellow and green in Fig. 4, are marked by consistent dash-colored lines in Fig. 5.

Although the estimated grain sizes are overestimated, especially when the crystallite sizes are small causing difficulty in reading the separation of the continuous diffraction spots across the azimuth, this visualization allows us to recognize the actual changes in microstructure as well as the corresponding mechanical property when the nanostructured metal experienced the elevated temperatures. Fig. 3(b) provides microstructural changes of up to 480 K corresponding to the recovery of the nanostructured Cu; Fig. 5 indicates further microstructural relaxation of recrystallization up to 700 K followed by grain growth, as also supported by the hardness drop. While the results are consistent with the hardness drop with a reduced dislocation density reported around 470 K of an HPT-processed Cu [21], where Fig. 4(b) shows the same results of the significant dislocation density drop around 470 K and higher, the present study comprehensively shows the series of recrystallization towards grain growth of the nanostructured Cu that

simultaneously and continuously changes the microstructural features, including dislocation density drop and microstrain reduction and crystallite increase, and mechanical properties over 700 K. Grain growth, accompanied by a further hardness reduction, is expected at such high temperatures, as supported by the reports on nanostructured Cu [22,23]. Regardless of additional treatment for microstructure stability, the nanostructure in Cu undergoes grain growth when heated at constant rates to temperatures over 800 K or higher, resulting in Cu grains of 4–5  $\mu\text{m}$  [24].

Microstructural characterization extends beyond microscopy. This high-energy synchrotron X-ray microbeam technique enables statistically robust characterization of nanoscale grains within the examined sample volume, capturing the evolution of various microstructural features [25], including lattice strain (Fig. 2), crystallite size, microstrain, and dislocation density (Fig. 4b) in nanostructured Cu during recrystallization in this study. The present work demonstrates the feasibility of the in situ heating diffraction technique to track continuous microstructural relaxation and provide quantitative and qualitative information from nanostructure to coarsening. It is worth noting that the Williamson Hall methods lead to grain sizes measured by diffraction, which is the coherent crystal volume of not too many distortions, i.e. the undistorted volume within dislocation cells or subgrains, leading here to circa 50 nm at 500 K. This increase from 40 nm at room temperature demonstrates a recovery process, mostly before recrystallization. The spot-counting method leads to the grain size, which integrates over dislocation cells and subgrains and, therefore, starts about one order of magnitude higher than the values obtained by Williamson-Hall. The trend of the high-temperature grain size is evident and has not been reported in such detail before.

#### 4.3. Stored energies necessary for defect-driven relaxation

It is essential to quantify the driving force of the recrystallization process in nanostructured Cu processed by severe plastic deformation by estimating the stored energy from various defects using microstructural data. Specifically, excess dislocations, grain boundaries, and vacancies created during nanostructuring by HPT are expected to significantly contribute to the total stored energy. First, elastic strain energy of dislocations per mass  $W_{\text{dis}}$  is estimated by,

$$W_{\text{dis}} = E_{\text{dis}} \cdot (\rho / \rho_m) \quad (1)$$

where  $E_{\text{dis}}$  denotes the strain energy per unit length of the dislocation, thus  $E_{\text{dis}} \cdot \rho$  yields the energy per volume, and  $\rho_m$  is mass-density of 8940  $\text{kg}/\text{m}^3$  for Cu [26]. The value of  $E_{\text{dis}}$  is estimated here by using the general term [27]:

$$E_{\text{dis}} = \left( f + \frac{1-f}{1-\nu} \right) \frac{Gb^2}{4\pi} \ln \left( \frac{1}{b\sqrt{\rho}} \right) \quad (2)$$

where shear modulus of  $G = 48 \text{ GPa}$ ,  $\rho = 6.8 \times 10^{14} \text{ m}^{-2}$  observed at 300 K in Fig. 4(b), and a Poisson's ratio of  $\nu = 0.34$  [26] are applied for Cu. Taking the equal fractions of screw dislocation  $f$  and edge dislocations  $1-f$  in the sample,  $W_{\text{dis}} = 120 \text{ J/kg}$  is computed for the nanostructured Cu. The computed value is smaller than the reported values of 200–300 J/kg for ECAP-processed Cu showing twice-high dislocation densities observed by lab-scale XRD [28]. Second, stored energy by grain boundary  $W_{\text{GB}}$  considers the involvement of high-angle grain boundaries. Applying the grain boundary energy of Cu after grain refinement processes  $\gamma_{\text{GB}} = 0.55 \text{ J/m}^2$  [29],  $W_{\text{GB}}$  is estimated by,

$$W_{\text{GB}} = 3\gamma_{\text{GB}} / (D \cdot \rho_m) \quad (3)$$

where  $D$  is the grain size of 240 nm after the grain refinement process observed by TEM in Fig. 1(a) for the present case. Thus,  $W_{\text{GB}}$  of  $\sim 770 \text{ J/kg}$  is estimated for the nanostructured Cu, which is supported by a similar value of  $630 \pm 80 \text{ J/kg}$  for high-angle grain boundaries of Cu

after HPT [13] and 650 J/kg of Cu after ECAP [30].

Third, the energy stored by vacancies  $W_{\text{vac}}$  can be estimated by the form,

$$W_{\text{vac}} = c_v E_f \left( \frac{N_A}{M} \right) \quad (4)$$

where  $c_v$  is a vacancy concentration,  $E_f$  is an estimated vacancy formation energy,  $N_A$  is Avogadro's number, and  $M$  is the molar mass. Considering the lattice strain relaxation model [31], a monovacancy in an f.c.c. crystal creates a volume change  $(V_0 - V_f) / V_0$ , where  $V_f$  and  $V_0$  are vacancy formation volume and atomic volume, respectively. The volumetric strain by a vacancy can be estimated by three times the linear lattice strain due to vacancy  $\Delta\varepsilon_v$ , and we assume the strained volume will affect the total unit cells of the neighbors of  $4^3$  per vacancy [8,32]. This provides  $c_v = 3\Delta\varepsilon_v / \{(1 - V_f/V_0) \times 4^3\} = 2.34 \times 10^{-4}$ , when applying  $V_f/V_0 = 0.80$  for a monovacancy in Cu crystals [31] and  $\Delta\varepsilon_v \approx 1 \times 10^{-3}$  referencing a linear lattice strain change due to the vacancy relaxation in an f.c.c. metal [33]. The estimated  $c_v$  agrees with the  $c_v$  values obtained from positron annihilation spectroscopy, electrical resistivity, differential scanning calorimetry, and time-differential dilatometry [34] ranging in the orders of  $10^{-4}$ – $10^{-3}$  on bulk nanostructured Cu after HPT [4,14] and ECAP [3,28,35,36]. Applying  $E_f$  of 1.27 eV [31] and  $M$  of 63.55 g/mol for Cu,  $W_{\text{vac}}$  of 450 J/kg is estimated for the nanostructured Cu. The total stored energy from these defects is approximately 1340 J/kg with  $W_{\text{GB}} > W_{\text{vac}} > W_{\text{dis}}$  for the nanostructured Cu. The hierarchy of stored energies,  $W_{\text{GB}} > W_{\text{vac}} > W_{\text{dis}}$ , agrees with a recent result on a nanostructured CoCrFeNi high-entropy alloy examined using in situ heating neutron experiments, where the total stored energy from the defects was estimated to be  $\sim 8500 \text{ J/kg}$  [33]. While limited studies estimated the stored energy associated with individual lattice defect, more data on stored energies from the defects and other microscopic features, e.g. residual stress, are necessary for various materials to understand the defect-driven microstructure behavior of these materials prepared by different manufacturing and processing techniques. The present study provides key insights into the overall driving forces of major defects by estimating the total stored energy contributing to the thermal relaxation processes of nanostructured metals, particularly highlighting the incorporation of the stored energy by excess vacancies. As noted earlier, measuring vacancies necessitates specialized advanced techniques. Additional experiments are needed to precisely determine the vacancy concentration in materials, which is particularly important for nanostructured materials subjected to severe deformation.

## 5. Summary and conclusions

The nanostructured Cu after HPT was examined for its microstructural evolution driven by excess defects using an in situ heating high-energy synchrotron microbeam X-ray. The following results are yielded from the novel diffraction experiment and analysis.

- (1) Average grain sizes of 240–260 nm were recorded by TEM. The peak shift tracked from the diffraction data shown in the intensity - scattering vector - time map determined an average thermal expansion coefficient of  $17.033 \times 10^{-6} \text{ K}^{-1}$  at a range of 303–361 K.
- (2) The study identified critical temperatures of the key microstructural transition: recovery transitioning to recrystallization around 470 K, followed by the onset of grain growth dominating above 700 K. These transitions were accompanied by variations in crystallite size, lattice strain, and dislocation density. It proves the feasibility of the diffraction technique to track continuous microstructural relaxation from nanostructure to coarsening.
- (3) An azimuth angle - time plot of the diffraction data for a specific reflection peak, such as Cu-111, was used to visualize the

transition of the microstructure under heating. Diffraction-data based grain size was estimated during the analysis, which also proves the consistent transition temperatures for the different microstructural relaxation behaviors from the nanostructured Cu after HPT.

- (4) The total stored energies, estimated to be 1340 J/kg, shows  $W_{GB} > W_{vac} > W_{dis}$  for the nanostructured Cu, highlighting the significant role of defects as a driving force behind these microstructural changes.

#### CRediT authorship contribution statement

**Bhatta Laxman:** Investigation, Formal analysis. **Lee Isshu:** Investigation, Formal analysis. **Kawasaki Megumi:** Writing – original draft, Supervision, Resources, Funding acquisition. **Lienert Ulrich:** Writing – review & editing, Methodology. **Liss Klaus-Dieter:** Writing – review & editing, Investigation, Formal analysis, Data curation, Conceptualization. **Xu Donghua:** Methodology. **Blankenburg Malte:** Methodology.

#### Declaration of Competing Interest

The authors declare that they have no known competing financial interests or personal relationships that could have appeared to influence the work reported in this paper.

#### Acknowledgements

This study was supported in part by the National Science Foundation of the United States under Grant No. CMMI-2051205 (M.K.). The authors acknowledge DESY (Hamburg, Germany), a member of the Helmholtz Association HGF, for the provision of experimental facilities. Parts of this research were carried out at the PETRA III beamline P21.2. Beamtime was allocated for proposal number I 20200639.

#### Appendix A. Supporting information

Supplementary data associated with this article can be found in the online version at doi:10.1016/j.jallcom.2025.180599.

#### Data availability

The data that support the findings of this study are available from the corresponding author on reasonable request.

#### References

- [1] X. Sauvage, G. Wilde, S.V. Divinski, Z. Horita, R.Z. Valiev, Grain boundaries in ultrafine grained materials processed by severe plastic deformation and related phenomena, *Mater. Sci. Eng. A* 540 (2012) 1–12, <https://doi.org/10.1016/j.msea.2012.01.080>.
- [2] R.Z. Valiev, R.K. Islamgaliev, I.V. Alexandrov, Bulk nanostructured materials from severe plastic deformation, *Prog. Mater. Sci.* 45 (2000) 103–189, [https://doi.org/10.1016/S0079-6425\(99\)00007-9](https://doi.org/10.1016/S0079-6425(99)00007-9).
- [3] E. Schafner, G. Steiner, E. Korznikova, M. Kerber, M.J. Zehetbauer, Lattice defect investigation of ECAP-Cu by means of X-ray line profile analysis, calorimetry and lectrical resistometry, *Mater. Sci. Eng. A* 410 (2005) 169–173, <https://doi.org/10.1016/j.msea.2005.08.070>.
- [4] J. Čížek, M. Janeček, T. Vlasák, B. Smola, O. Melikhova, R.K. Islamgaliev, S. V. Dobatkin, The development of vacancies during severe plastic deformation, *Mater. Trans.* 60 (2019) 1533–1542, <https://doi.org/10.2320/matertrans.MF201937>.
- [5] I. Bibimoune, E. Hirschmann, M.O. Liedke, A. Wagner, M. Kawasaki, T. Baudin, I. Mkinci, K. Abib, Y. Huang, T.G. Langdon, D. Bradai, Defect microstructure evolution in an immiscible composite Cu43% Cr alloy after high-pressure torsion and annealing using positron annihilation spectroscopy, *Met. Mater. Inter* (2024), <https://doi.org/10.1007/s12540-024-01745-2>.
- [6] H.R. Peng, M.M. Gong, Y.Z. Chen, F. Liu, Thermal stability of nanocrystalline materials: thermodynamics and kinetics, *Int. Mater. Rev.* 62 (2016) 303–333, <https://doi.org/10.1080/09506608.2016.1257536>.
- [7] K. Edalati, Z. Horita, Universal plot for hardness variation in pure metals processed by high-pressure torsion, *Mater. Trans.* 51 (2010) 1051–1054, <https://doi.org/10.2320/matertrans.M2009431>.
- [8] K.D. Liss, J.K. Han, M. Blankenburg, U. Lienert, S. Harjo, T. Kawasaki, P.G. Xu, E. Yukutake, M. Kawasaki, Recrystallization of bulk nanostructured magnesium alloy AZ31 after severe plastic deformation: an in situ diffraction study, *J. Mater. Sci.* 59 (2024) 5831–5853, <https://doi.org/10.1007/s10853-023-09250-4>.
- [9] T. Konkova, S. Mironov, A. Korznikov, S.L. Semiatin, Microstructure instability in cryogenically deformed copper, *Scr. Mater.* 63 (2010) 921–924, <https://doi.org/10.1016/j.scriptamat.2010.07.005>.
- [10] Y. Huang, S. Sabbaghianrad, A.I. Almazroue, K.J. Al-Fadhlah, S.N. Alhajeri, T. G. Langdon, The significance of self-annealing at room temperature in high purity copper processed by high-pressure torsion, *Mat. Sci. Eng. A* 656 (2016) 55–66, <https://doi.org/10.1016/j.msea.2016.01.027>.
- [11] P. Král, J. Staněk, L. Kuncická, F. Seitl, L. Petrich, V. Schmidt, V. Beneš, V. Sklenička, Microstructure changes in HPT-processed copper occurring at room temperature, *Mater. Charact.* 151 (2019) 602–611, <https://doi.org/10.1016/j.matchar.2019.03.046>.
- [12] J. Gubicza, S.V. Dobatkin, E. Khosravi, A.A. Kuznetsov, J.L. Labar, Microstructural stability of Cu processed by different routes of severe plastic deformation, *Mater. Sci. Eng. A* 528 (2011) 1828–1832, <https://doi.org/10.1016/j.msea.2010.11.026>.
- [13] P. Jenei, J. Gubicza, E.Y. Yoon, H.S. Kim, J.L. Labar, High temperature thermal stability of pure copper and copper-carbon nanotube composites consolidated by High Pressure Torsion, *Compos. Part A-Appl. S.* 51 (2013) 71–79, <https://doi.org/10.1016/j.compositesa.2013.04.007>.
- [14] J. Čížek, M. Janeček, O. Srba, R. Kuzel, Z. Barnovská, I. Procházka, S. Dobatkin, Evolution of defects in copper deformed by high-pressure torsion, *Acta Mater.* 59 (2011) 2322–2329, <https://doi.org/10.1016/j.actamat.2010.12.028>.
- [15] K. Edalati, T. Fujioka, Z. Horita, Microstructure and mechanical properties of pure Cu processed by high-pressure torsion, *Mat. Sci. Eng. A* 497 (2008) 168–173, <https://doi.org/10.1016/j.msea.2008.06.039>.
- [16] U. Vainio, K. Pirkkalainen, K. Kisko, G. Goerigk, N.E. Kotelnikova, R. Serimaa, Copper and copper oxide nanoparticles in a cellulose support studied using anomalous small-angle X-ray scattering, *Eur. Phys. J. D.* 42 (2007) 93–101, <https://doi.org/10.1140/epjd/e2007-00015-y>.
- [17] T.A. Hahn, Thermal expansion of copper from 20 to 800 K—standard reference material 736, *J. Appl. Phys.* 41 (13) (1970) 5096–5101, <https://doi.org/10.1063/1.1658614>.
- [18] T. Ungár, Characterization of nanocrystalline materials by x-ray line profile analysis, *J. Mater. Sci.* 42 (5) (2006) 1584–1593, <https://doi.org/10.1007/s10853-006-0696-1>.
- [19] M.B. Kerber, M.J. Zehetbauer, E. Schafner, F.C. Spieckermann, S. Bernstorff, T. Ungar, X-ray line profile analysis—an ideal tool to quantify structural parameters of nanomaterials, *JOM* 63 (2011) 61–70, <https://doi.org/10.1007/s11837-011-0115-1>.
- [20] G.K. Williamson, R.E. Smallman, III. Dislocation densities in some annealed and cold-worked metals from measurements on the x-ray debye-scherrer spectrum, *Philos. Mag.* 1 (1956) 34–46, <https://doi.org/10.1080/14786435608238074>.
- [21] P. Cengeri, M.B. Kerber, E. Schafner, M.J. Zehetbauer, D. Setman, Strengthening during heat treatment of HPT processed copper and nickel, *Mat. Sci. Eng. A* 742 (2019) 124–131, <https://doi.org/10.1016/j.msea.2018.11.010>.
- [22] R.A. Andrievski, Review of thermal stability of nanomaterials, *J. Mater. Sci.* 49 (2014) 1449–1460, <https://doi.org/10.1007/s10853-013-7836-1>.
- [23] F. Khodabakhshi, M. Mohammadi, A.P. Gerlich, Stability of ultra-fine and nano-grains after severe plastic deformation: a critical review, *J. Mater. Sci.* 56 (2021) 15513–15537, <https://doi.org/10.1007/s10853-021-06274-6>.
- [24] X.Y. Li, X. Zhou, K. Lu, Rapid heating induced ultrahigh stability of nanograined copper, *Sci. Adv.* 6 (17) (2020) eaaz8003, <https://www.science.org/doi/10.1126/sciadv.aaz8003>.
- [25] M. Kawasaki, J.-K. Han, X. Liu, S.-C. Moon, K.-D. Liss, Synchrotron high-energy x-ray & neutron diffraction, and laser-scanning confocal microscopy: in-situ characterization techniques for bulk nanocrystalline metals, *Mater. Trans.* 64 (2023) 1683–1694, <https://doi.org/10.2320/matertrans.MT-MF2022022>.
- [26] N.J. Simon, E.S. Drexler, R.P. Reed, Properties of copper and copper alloys at cryogenic temperatures. Final report, United States, 1992, <https://doi.org/10.2172/5340308>.
- [27] M.B. Bever, D.L. Holt, A.L. Titchener, The stored energy of cold work, *Prog. Mater. Sci.* 17 (1973) 5–177, [https://doi.org/10.1016/0079-6425\(73\)90001-7](https://doi.org/10.1016/0079-6425(73)90001-7).
- [28] J. Gubicza, S.V. Dobatkin, E. Khosravi, Reduction of vacancy concentration during storage of severely deformed Cu, *Mater. Sci. Eng. A* 527 (2010) 6102–6104, <https://doi.org/10.1016/j.msea.2010.05.088>.
- [29] X. Zhou, X.Y. Li, K. Lu, Enhanced thermal stability of nanograined metals below a critical grain size, *Science* 360 (2018) 526–530, <https://doi.org/10.1126/science.aar6941>.
- [30] N.N. Liang, Y.H. Zhao, Y. Li, T. Topping, Y.T. Zhu, R.Z. Valiev, E.J. Lavernia, Influence of microstructure on thermal stability of ultrafine-grained Cu processed by equal channel angular pressing, *J. Mater. Sci.* 53 (2018) 13173–13185, <https://doi.org/10.1007/s10853-018-2548-1>.
- [31] L.Y. Nemirovich-Danchenko, A.G. Lipnitskii, S.E. Kul'kova, Vacancies and their complexes in FCC metals, *Phys. Solid State* 49 (2007) 1079–1085, <https://doi.org/10.1134/S1063783407060108>.
- [32] D. Sahoo, H.K. Sahu, Lattice distortion around a vacancy in magnesium, *Phys. Rev. B* 18 (1978) 6738–6743, <https://doi.org/10.1103/PhysRevB.18.6738>.
- [33] X.J. Liu, J.K. Han, Y. Onuki, Y.O. Kuzminova, S.A. Evlashin, M. Kawasaki, K.D. Liss, In situ neutron diffraction investigating microstructure and texture evolution upon heating of nanostructured CoCrFeNi high-entropy alloy, *Adv. Eng. Mater.* 25 (2023) 2201256, <https://doi.org/10.1002/adem.202201256>.
- [34] R. Wurschum, B. Oberdorfer, E.M. Steyskal, W. Sprengel, W. Puff, P. Pikart, C. Hugenschmidt, R. Pippa, Free volumes in bulk nanocrystalline metals studied

- by the complementary techniques of positron annihilation and dilatometry, Phys. B Condens. Matter 407 (2012) 2670–2675, <https://doi.org/10.1016/j.physb.2012.01.090>.
- [35] T. Ungár, E. Schafler, P. Hanák, S. Bernstorff, M. Zehetbauer, Vacancy production during plastic deformation in copper determined by in situ x-ray diffraction, Mat. Sci. Eng. A 462 (2007) 398–401, <https://doi.org/10.1016/j.msea.2006.03.156>.
- [36] M. Zehetbauer, E. Schafler, T. Ungár, Vacancies in plastically deformed copper, Int. J. Mater. Res. 96 (2022) 1044–1048, <https://doi.org/10.1515/ijmr-2005-0180>.